Semiconductor Physics, Quantum Electronics & Optoelectronics, 2017. V. 20, N 4. P. 418-423.
doi: https://doi.org/10.15407/spqeo20.04.418

PACS 68.37.Ps, 73.40.-c

Macroscopic versus microscopic photovoltaic response of heterojunctions based on mechanochemically prepared nanopowders of kesterite and *n*-type semiconductors

O.P. Dimitriev[1], D.O. Grynko[1], A.M. Fedoryak[1], T.P. Doroshenko[1], M. Kratzer[2], C. Teichert[2], Yu.V. Noskov[3], N.A. Ogurtsov[3], A.A. Pud[3], P. Balaz[4], M. Balaz[4], M. Tesinsky[4]
[1]*V. Lashkaryov Institute of Semiconductor Physics of NAS of Ukraine, 45, prospect Nauky, 03680 Kyiv, Ukraine*
[2]*Institut für Physik, Montanuniversität Leoben, Franz-Josef-Straße 18, Leoben A-8700, Austria*
[3]*Institute of Bioorganic Chemistry and Petrochemistry, NAS of Ukraine, 50, Kharkivske Shose, 02160 Kyiv, Ukraine*
[4]*Institute of Geotechnics, Slovak Academy of Sciences, 45, Watsonova str., Kosice 04010, Slovakia*

Abstract. Mechanochemically prepared nanopowder of selenium-free kesterite Cu_2ZnSnS_4 (CZTS) in combination with *n*-type semiconductors, *i.e.*, CdS, ZnO and TiO_2, was tested in planar and bulk-heterojunction solar cells. The samples have been studied by macroscopic current-voltage (*I-V*) measurements and Kelvin-probe atomic-force microscopy (KPFM). KPFM images taken under light illumination showed the distribution of the potential across the surface, with negative potential on the *n*-type semiconductor domains and positive potential on the CZTS domains, which indicated charge separation at the interface of the counterparts. The best result was found for the CdS-CZTS composition, which showed a potential difference between the domains up to 250 mV. These results were compared with the planar heterojunctions of CdS/CZTS and TiO_2/CZTS, where CZTS nanopowder was pressed/deposited directly onto the surface of films of the corresponding *n*-type semiconductors. Again, *I-V* characteristics showed that cells based on CdS/CZTS heterojunctions have the best performance, with a photovoltage up to 200 mV and photocurrent densities up to 0.1 mA/cm^2. However, the carrier generation was found to occur mainly in the CdS semiconductor, while CZTS showed no photo-response and served as the hole-transporting layer only. It is concluded that sensitization of the kesterite powder obtained by mechanochemical method is necessary to improve the performance of the corresponding solar cells.

Keywords: kesterite, cadmium sulphide, nanopowder, bulk heterojunction, photovoltaics.

Manuscript received 02.11.17; revised version received 21.11.17; accepted for publication 07.12.17; published online 07.12.17.

1. Introduction

Photovoltaic (PV) cells based on bulk heterojunctions (BHJs) of electron-donor and electron-acceptor components are developing for the last decades and have attracted great attention as they provide some advantages compared to the traditional bilayer geometry of donor-acceptor or *p*-type/*n*-type semiconductor heterojunctions. The main advantage of the BHJ geometry is an increased interface area between the components and thus the total increased amount of charge separated carriers at the interface upon light illumination.

Various combinations of donor and acceptor materials have been used to produce BHJ solar cells. The most known ones include organic-organic, such as poly(3-hexylthiophene) (P3HT)– fullerene derivative

PCBM [1-3], copper phthalocyanine (PcCu) – fullerene C60 [4, 5] and hybrid organic-inorganic combinations, such as P3HT-CdSe nanocrystals [6, 7], dye-sensitized TiO_2 particle cells [8, 9], as well as inorganic-inorganic, e.g., CdSe-CdTe nanoparticle [10] combinations, *etc*.

Kesterites are relatively new materials for application in solar cells, which have attracted considerable attention in recent years [11]. Kesterite is a promising material with a potential to replace $Cu(In,Ga)Se_2$ (CIGS) and related alloys. Compared to CIGS, this material exhibits a reduced toxicity and greater abundance of the constituent elements. The quaternary semiconductor compound kesterite, Cu_2ZnSnS_4 (CZTS), is known as an effective absorber material, which possesses an optimal direct band gap of ~1.5 eV, a high absorption coefficient of $\sim 10^4$ cm^{-1} and a power conversion efficiency in respective solar cells to be as high as 12.6% [12, 13]. However, the CZTS production technology relies on high temperature annealing (~500 °C) under the chalcogen atmosphere and/or toxic hydrazine-based methodologies, which is the drawback of this material. Recently, the environmentally friendly ball milling method utilizing tools of mechanochemistry was applied for the synthesis of kesterites [14-16], which allows one to prepare the powder with particles as small as few nanometers in size. Additional benefit of using the CZTS nanopowder is that it can be readily used in BHJ solar cells. In this work, we study applicability of mechanochemically prepared kesterite nanopowders in planar and BHJ solar cells.

2. Experimental

2.1. Sample preparation

CZTS nanopowder (average crystallite size 7–8 nm) was prepared by co-milling of stoichiometric amounts of copper (99% Merck, Germany), zinc (99% Aldrich,Germany), tin (Nihon Seiko, Japan) and sulfur (99% CG-Chemikalien, Germany). For the mechanochemical synthesis, an industrial eccentric vibratory ball mill ESM 656-0.5 ks (Siebtechnik, Germany) working under the following conditions was used: 5L steel satellite milling chamber attached to the main corpus of the mill, tungsten carbide balls with a diameter of 35 mm with a total mass 30 kg, 80% ball filling, amplitude of the mill 20 mm, rotational speed of the eccenter 960 min^{-1}, argon atmosphere, the feed 100 g, milling time 360 min. The samples were prepared in the form of the pressed pellets followed by measurement of their density and specific resistivity.

Three n-type semiconductor powders, *i.e*., CdS microcrystals (99.9%, 1–20 μm, Ukraine), ZnO nanocrystals (99.9%, ~30 nm, MTI Corporation, CA) and TiO_2 nanocrystals (anatase 99.99%, 5–10 nm, MTI Corporation, CA) have been selected to prepare planar or bulk heterojunctions with CZTS by pressing the mixtures (1:1 weight ratio) in a capillary tube of 1 mm in diameter. For planar heterojunctions the CZTS pellet was compressed directly on the surface of a CdS sample with a Fe rod served as the top electrode.

Hybrid solar cells based on TiO_2/CZTS heterojunctions were prepared by subsequent deposition of the layers on conductive fluorine doped tin oxide (FTO)/glass substrates (20.5×25 mm, resistance 8 Ohm/sq, Solaronix, Switzerland). In particular, FTO substrates were precleaned by ultrasonication subsequently in acetone and isopropyl alcohol baths for 3 min. At the next cleaning stages, these substrates were washed with distilled water followed by 5 min boiling in 30% H_2O_2 bath; then washed again and dried. These substrates were then coated with TiO_2 porous layer as follows. 200 mg of TiO_2 nanopowder (Degussa P25) were ground with a few drops of acetic acid (mixture of 10 μl of glacial acetic acid with 5 ml of water) and 1 drop of a detergent in an agate mortar. The prepared paste was screen-printed on the cleaned FTO substrates which were then annealed on a heating plate at ~450 °C for 20 minutes and left to cool down to ambient temperature. The formed TiO_2 layer was drop-coated with a dispersion of CZTS (2 mg of CZTS/100 μl of chlorobenzene, prepared for 30 min of ultrasonication), then dried at 40 °C. This CZTS layer was drop-coated with 50 μl of P3HT solution (2 mg of P3HT/100 μl of chlorobenzene) and then dried at 40 °C. Finally, Ag contacts were deposited on the P3HT layer surface using a silver paint, followed by drying the sample at 80 °C.

2.2. Characterization

The specific resistivity of the pressed pellets of kesterite nanopowder was measured by a two-probe method as follows. The powder was loaded to a capillary tube and then compressed with a pressure of up to 10 kg/mm^2 from the both sides by iron rods connected to the tester until the resistance has reached its saturation value. The tube was weighted before and after the powder load in order to calculate the mass m of the loaded powder. From the above data, the density d and specific resistivity r have been calculated as follows:

$$d = m/lS,$$

$$r = R{\cdot}S/l,$$

where S is the cross sectional area of the capillary hole, l – height of the compressed pellet, R – measured resistance.

A hot-probe method has been used to determine the type of conductivity of the materials. In this method, the sample is locally heated from one edge, while measuring potential difference between the hot and the cold edges of the sample. Charge carriers diffuse from the hot to the cold edge, and majority of the carriers (electrons or holes) determines the sign of the potential difference.

Current-voltage (*I-V*) measurements were employed to study macroscopic PV performance of the prepared solar cell structures. *I-V* measurements were done by using a HP 4140B source-meter device. The active area of the samples was several square millimeters, and white light illumination of the samples was provided using the 50 W halogen lamp. The results below are referred to light illumination of ~1000 W/m^2.

Kelvin-probe atomic force microscopy (KPFM) [17] and conductive atomic force microscopy (CAFM) [18] were used to study microscopic arrangement of *n*- and *p*-type regions in bulk heterojunctions as well as to study a map of local photocurrents in the samples. For these studies an Asylum Research MFP 3D System was used with nitrogen doped diamond probes (DCP-11 from NT-MDT, r_{tip} ~ 100 nm, k ~5.5 N/m, resistivity of coating ~0.5–1 Ω·cm). The samples were studied in the dark and under white light illumination of ~120 W/m^2.

3. Results and discussion

3.1. CZTS properties

The measured density and conductivity of the pressed pellets of the synthesized CZTS nanopowder are shown in Table 1. The density of the pellets can be also compared to the tabulated values of the natural minerals, *i.e*., 4.56 g/cm^3 for kesterite [19]. From the above data, it can be seen that the kesterite nanopowder was compressed under the applied pressure practically to the tightly-packed material. This was confirmed through unloading of the material from the capillary tube. Upon unloading, the pellet kept its form as a single, compact piece without cracking.

The hot-probe method was used to determine the type of conductivity using the above tube loaded with the nanopowder. The synthesized material revealed *p*-type behavior. However, it should be noted that the synthesized samples of kesterite did not show any photosensitivity, *i.e*., the changes in resistivity upon illumination, which is not typical for solar cell materials.

3.2. Macroscopic studies of PV response

3.2.1. PV cells based on CdS/CZTS heterojunctions

PV structures created by subsequent mechanical pressuring of the layers one on the other cannot be considered as a viable approach for application due to poor contact between the layers, but it rather serves as a model system to evaluate the applicability of the material combination for its further optimization in the future structures. Moreover, because of poor control of the interface area, PV parameters can strongly vary from sample to sample. The typical synthesized in this work heterostructure of In/CdS/Kesterite/Fe, showed an open-circuit voltage of U_{oc} = 60 mV, photocurrent density J_{sc} = 40 μA/cm^2, fill factor FF = 0.25, and overall power conversion efficiency PCE = $6\cdot10^{-4}$% (Fig. 1 and Table 2). The relatively poor performance can be explained as mainly arising from an uncontrollable contamination of the interface during pellet handling and pressing, and poor contact of CZTS pellet to the CdS surface. Interface contamination leads to reduced open-circuit voltage and fill factor, and poor contact leads to reduced photocurrent, respectively. In fact, the photocurrent passways are limited by a few contact points at the rough interface. Therefore, the true photocurrent density is much higher taking into account that the effective interface area composed of the contacting nanoparticles, through which the current is passing, is much less compared to the macroscopic area of the pellet. For example, it was found that PV performance can be improved by increasing the pressure at the interface, implying that the effective interface area increases. At high pressure, the open-circuit voltage and photocurrent density can be increased up to 200 mV and 100 μA/cm^2, respectively.

Table 1. Density and electrical characteristics of CZTS pellets.

Density	4.55 g/cm^3
Specific resistivity	4.85 Ohm·cm
Conductivity	0.21 S/cm

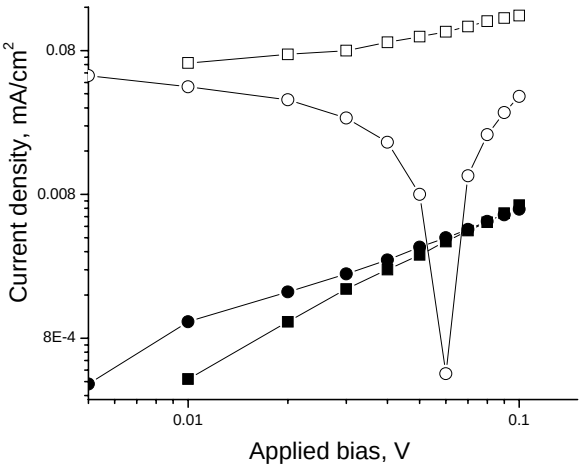

Fig. 1. *I-V* characteristics of In/CdS/Kesterite/Fe heterostructure in the darkness (filled symbols) and under illumination (open symbols): circles correspond to negative and squares to positive bias on In.

Table 2. PV parameters of the heterostructures used in this study.

Heterostructure	J_{sc}, mA/cm^2	U_{oc}, mV	FF	PCE, %
In/CdS/Kesterite/Fe	$4.0\cdot10^{-2}$	60	0.25	$6.0\cdot10^{-4}$
FTO/TiO2/Kesterite/ P3HT/Ag	$7.6\cdot10^{-5}$	190	0.25	$3.6\cdot10^{-6}$

It was found that filtering out of the spectral range of light illumination by long-pass filter with the cut-on wavelength at ~550 nm results in a substantial suppression of the PV response of the heterostructure. Such a suppression points out that the major contribution to the PV response comes from CdS, the band gap of which is at 2.42 eV (513 nm), while CZTS with the band gap of about 1.5 eV serves as a hole-transporting layer only.

3.2.2. PV cells based on TiO_2 /CZTS heterojunctions

The structure of FTO/TiO_2/kesterite/P3HT/Ag showed rather poor PV performance (Fig. 2), which was mainly limited by the low photocurrent and fill factor (Table 2). In addition to the problems discussed above for the CdS/kesterite heterojunction, the low photocurrent is explained here by the high resistivity of the TiO_2 layer, and the overall low performance is also caused by the absence of absorption of TiO_2 layer in the visible region, whereas the kesterite layer is not photoactive, as discussed above.

3.3. Microscopic studies of PV response

The surfaces of the pellets of BHJ mixtures were investigated using KPFM and CAFM in the dark and under illumination. It was found that all three heterojunctions based on CdS/CZTS, ZnO/CZTS and TiO_2/CZTS possessed a response to light, changing the surface potential upon illumination. However, the strongest photoresponse was obtained for the CdS/CZTS mixture, where changes in the contact potential difference between dark and illuminated surface of up to 250 mV occurred (Fig. 3, lower panel), while ZnO/CZTS (Fig. 3, upper panel) and TiO_2/CZTS structure (not shown) showed very poor photo-response.

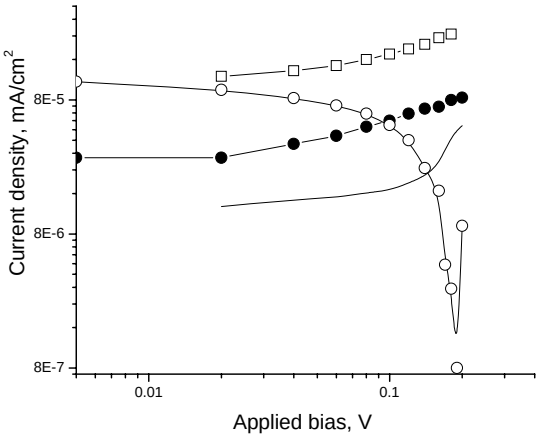

Fig. 2. *I-V* characteristics of FTO/TiO_2/kesterite/P3HT/Ag heterostructure in the darkness (filled symbols) and under illumination (open symbols): circles correspond to negative and squares to positive bias on FTO.

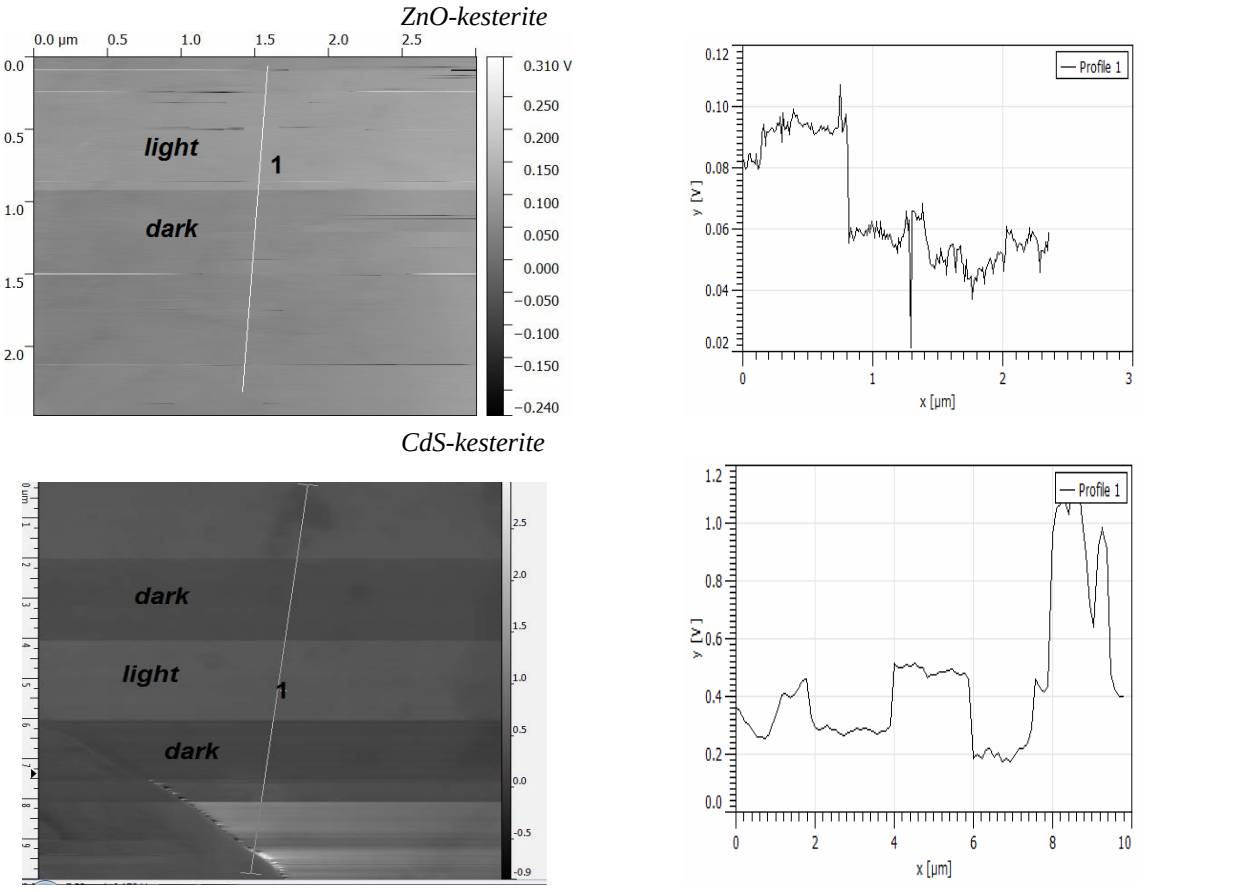

Fig. 3. KPFM potential map under dark-light switch (left panel) and surface potential changes along the line 1 for ZnO-kesterite (upper row) and CdS-kesterite (low row) samples.

In order to understand contribution of the components to the photo-response, the neat CdS and kesterite samples were studied separately. Firstly, it was found that the potential sign on the cantilever measured with respect to the CdS surface is always positive, whereas it is negative in respect to the kesterite surface (Fig. 4). Secondly, a significant response to light for the neat CdS sample was obtained ($\Delta CPD = -320 \pm 19$ mV), whereas no response to light for the kesterite sample was measured, which was within the experimental error ($\Delta CPD = -30 \pm 50$ mV, Fig. 4). Thus, we can conclude that the major response to light illumination in BHJ mixtures comes from the CdS domains (Fig. 3). Moreover, the average shift of the signal in CdS domains upon illumination (~300 mV) is much higher than the open-circuit voltage measured macroscopically (within ~10…200 mV) even though the light illumination intensity in KPFM experiments was lower than in the macroscopic studies. That indicates that macroscopic PV performance can be increased potentially and that the macroscopic sample is not optimized on the microscopic level.

It should be noted that the above difference in the potential sign measured using KPFM from the different domains can be used to distinguish the component domains themselves in the BHJ structure. In addition to the opposite potential signs for the different components, the different domains can be distinguished also by their conduction behavior. CAFM studies showed that *I-V* characteristics measured on the different domains of CdS-kesterite BHJ structure indicate that the AFM probe-sample heterojunctions forms a diode (Fig. 5). However, the diode is open at a positive bias only for the cantilever-kesterite heterojunction (Fig. 5b), and it is open at a negative bias only for the cantilever-CdS heterojunction (Fig. 5a). Thus, *I-V* characteristics allow us to distinguish the different domains in the BHJ structure as well. The role of the AFM probe in the above effects is crucial and will be reported in a separate paper.

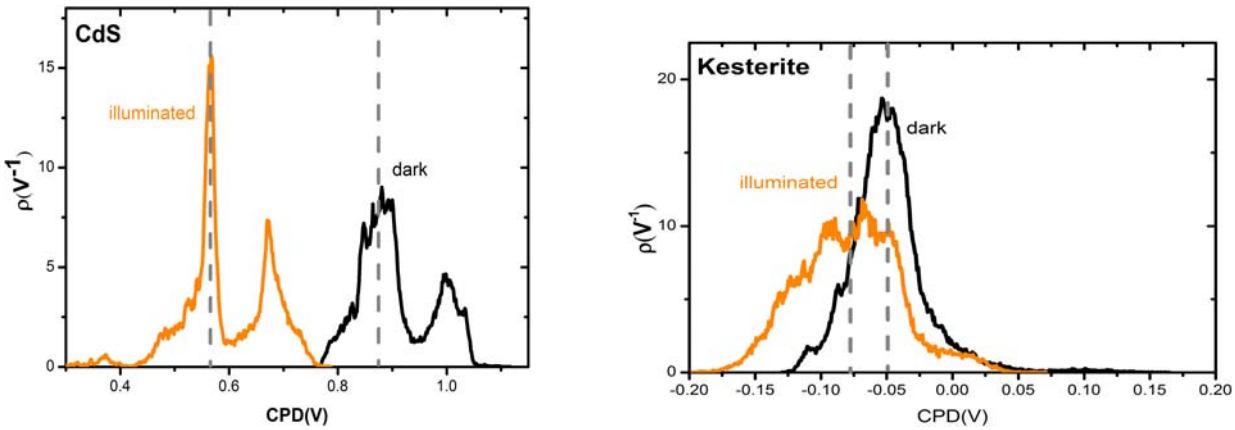

a b

Fig. 4. Average weight of KPFM signal depending on its value for (a) neat CdS and (b) neat kesterite sample.

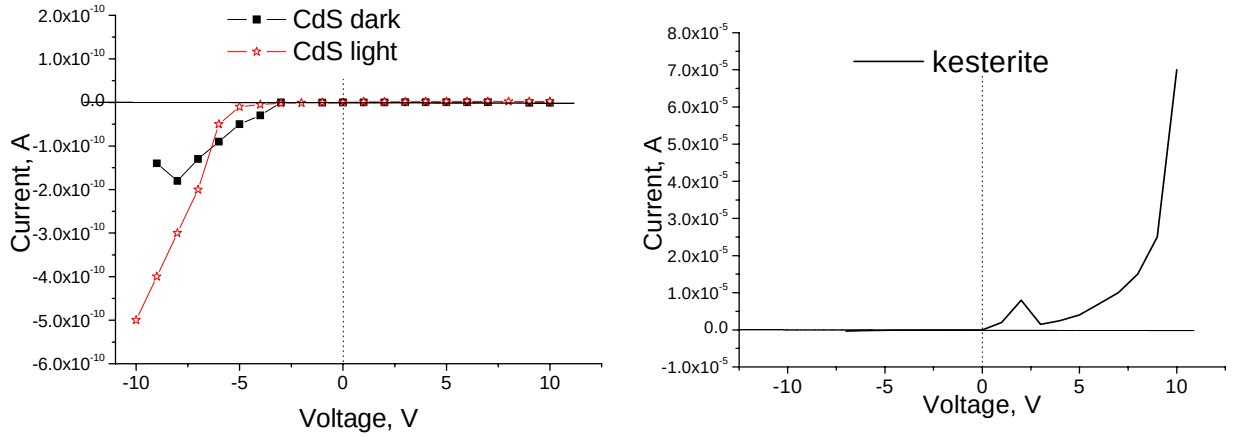

a b

Fig. 5. *I-V* curves from microscopic (a) CdS and (b) kesterite domains as measured by CAFM.

4. Conclusions

It was found that among binary compositions of ZnO-kesterite, TiO_2-kesterite and CdS- kesterite only the latter shows substantial response to white light. KPFM allows us to distinguish between the mechanochemically synthesized *p*-type kesterite and *n*-type CdS semiconductor micro-domains in bulk heterojunctions mixture: kesterite domains show the positive and CdS domains negative potential difference with respect to the AFM probe (N-doped diamond). CAFM (with the N-doped diamond AFM probe) also allowed us to distinguish between *p*-type kesterite and *n*-type CdS semiconductor micro-domains in BHJ mixture: *I-V* characteristics showed the diode behavior, but the kesterite-based diode is open at the positive bias, and the CdS-based diode at the negative bias, respectively. Thus, both KPFM and CAFM have a good potential in distinguishing *p*-type and *n*-type semiconductor domains in BHJ structures.

It was observed that the average shift of the signal in CdS domains upon illumination is much higher (~300 mV) than the open-circuit voltage measured macroscopically (~10…200 mV) even though the light illumination intensity in KPFM experiments (120 W/m^2) was significantly lower than in our macroscopic studies (1000 W/m^2). That indicates that macroscopic extraction of photocarriers proceeds not effectively, and overall PV performance can be increased substantially by proper optimization of the macroscopic sample on the microscopic level.

Acknowledgements

The work was supported by Ministry of Education and Science of Ukraine, Austrian Academic Exchange Service through the project UA 07/2015. and by the APVV Agency under the contract No. APVV-14-0103.

References

1. Thompson B.C., Frèchet J.M.J. Polymer–fullerene composite solar cells. *Angew. Chem. Intl. Ed*. 2008. **47**. P. 58–77.
2. Shaheen S.E., Brabec C.J., Sariciftci N.S. 2.5% efficient organic plastic solar cells. *Appl. Phys. Lett*. 2001. **78**. P. 841.
3. Jorgensen M., Norrman K. and Krebs F.C. Stability/degradation of polymer solar cells. *Sol. Energy Mater. Sol. Cells*. 2008. **92**. P. 686–714.
4. Uchida S., Xue J., Rand B.P., Forrest S.R. Organic small molecule solar cells with a homogeneously mixed copper phthalocyanine: C60 active layer. *Appl. Phys. Lett*. 2004. **84**. P. 4218.
5. Sullivan P., Heutz S., Schultes S.M., Jones T.S. Influence of codeposition on the performance of CuPc–C60 heterojunction photovoltaic devices. *Appl. Phys. Lett*. 2004. **84**. P. 1210.
6. Milleron D.J., Gur I., and Alivisatos A.P. Hybrid organic–nanocrystal solar cells. *MRS Bulletin*. 2005. **30**. P. 41–44.
7. Boucle J., Ravirajan P., Nelson J. Hybrid polymer–metal oxide thin films for photovoltaic applications. *J. Mater. Chem*. 2007. **17**. P. 3141–3153.
8. O'Regan B., Graetzel M. A low-cost, high-efficiency solar cell based on dye-sensitized colloidal TiO_2 films. *Nature.* 1991. **353**. P. 737–740.
9. Graetzel M. Dye-sensitized solar cells. *J. Photochem. Photobiol. C*. 2003. **4**. P. 145–153.
10. Gur I., Fromer N.A., Geier M.L., Alivisatos A.P. Air-stable all-inorganic nanocrystal solar cells processed from solution. *Science.* 2005. **310**. P. 462–465.
11. Mitzi D.B., Gunawan O., Todorov T.K., Wang K., Guha S. The path towards a high-performance solution-processed kesterite solar cell. *Sol. Energy Mater. Sol. Cells.* 2011. **95**. P. 1421–1436.
12. Persson C. Electronic and optical properties of Cu_2ZnSnS_4 and $Cu_2ZnSnSe_4$. *J. Appl. Phys.* 2010. **107**. P. 053710.
13. Wang W., Winkler M.T., Gunawan O., Gokmen T., Todorov T.K., Zhu Y., Mitzi D.B. Device characteristics of CZTSSe thin□film solar cells with 12.6% efficiency. *Adv. Energy Mater.* 2014. **4**. P. 1301465.
14. Wang Y., Gong H. Cu_2ZnSnS_4 synthesized through a green and economic process. *J. Alloys Compd*. 2011. **509**. P. 9627–9630.
15. Pareek D., Balasubramaniam K.R., Sharma P. Reaction pathway for synthesis of $Cu_2ZnSn(S/Se)_4$ via mechano-chemical route and annealing studies. *J. Mater. Sci. Mater. Electron.* 2017. **28**. P. 1199–1210.
16. Ritscher A., Schlosser M., Pfitzner A., Lerch M. Study of the mechanochemical process to crystalline Cu_2ZnSnS_4 powder. *Mater. Res. Bull*. 2016. **84**. P. 162–167.
17. Nonnenmacher M., O'Boyle M.P., Wickramasinghe H.K. Kelvin probe force microscopy. *Appl. Phys. Lett.* **58**, 2921-2923 (1991).
18. Teichert C., Beinik I. Conductive atomic force microscopy investigation of nanostructures in microelectronics, in: *Scanning Probe Microscopy in Nanoscience and Nanotechnology*, Vol. 2, ed. by B. Bhushan. Springer-Verlag, Berlin, 2011, P. 691–721.
19. http://www.webmineral.com/data/Kesterite.shtml